Supplementary Information

Ultrasmooth metal halide perovskite thin films via sol-gel processing

Ross A. Kerner*[a], Lianfeng Zhao [a], Zhengguo Xiao [a], and Barry P. Rand[a,b]

[a.] *Department of Electrical Engineering, Princeton University, Princeton, New Jersey 08544, United States*
[b.] *Andlinger Center for Energy and the Environment, Princeton University, Princeton, New Jersey 08544, United States*

Experimental

Materials and Perovskite Film Fabrication

MAI was synthesized by mixing aqueous methylamine (Sigma Aldrich) and aqueous HI (Sigma Aldrich, stabilized) solutions together. Butylammonium iodide (BAI) was synthesized by reacting butylamine (Sigma Aldrich) with equimolar amount of aqueous HI (Sigma Aldrich, stabilized). Butylammonium bromide was synthesized with the same procedure. The alkylammonium halides were washed with an ethanol:ether solvent mixture and rotovaped several times to remove the HI stabilizer. Precursor solutions were prepared by mixing lead halides (Sigma Aldrich, ≥ 98%) and methylammonium halide powders in a 1:1 molar ratio (plus the butylammonium halide additive if applicable) with N,N-dimethylformamide (DMF, Sigma Aldrich, 99.8% anhydrous) in a single vial to obtain the desired concentrations. Concentrated PbI_2 solutions (≥ 500 mg/mL) in DMF were not stable and require moderate heating and stirring to dissolve. Solutions were allowed to stir for at least 30 minutes. Inorganic $CsPbBr_3$ (CsBr from Sigma Aldrich, 99.9%) solutions were prepared in dimethyl sulfoxide (DMSO, Sigma Aldrich, 99.9%) at 0.5 M concentration and stirred overnight. Films were spin coated onto clean, O_2 plasma treated glass slides. A 200 nm PTFE filter was used to remove large aggregates prior to spinning. The toluene

application technique for the solvent exchange, similar to the technique from Ref. 1, was used to vary the film morphology for the methylammonium perovskites and chloroform was used for the solvent exchange with DMSO for the cesium perovskite films. All film fabrication was done in a glovebox with an N_2 atmosphere to remove the effects of humidity.

Film Characterization

The surface morphology and domain sizes of the films were imaged by tapping mode atomic force microscopy (AFM) using a Veeco diInnova large area scanner and a Quanta Environmental scanning electron microscope (SEM) at low acceleration voltages (~10 kV) and 0.8 Torr to avoid charging. Contact mode AFM was used for $CsPbBr_3$ films since the attractive potential for the AFM tip was unusually strong and deflected the tapping tip so much as to produce only low fidelity images. Particle sizes in the solutions were characterized by dynamic light scattering (DLS) using a Malvern ZetaSizer Nano ZS. The DLS data collection was performed on solutions in a quartz cuvette using a 632 nm laser with a 173° non-invasive backscatter detector. Analysis was carried out with ZetaSizer software version 7.11 using the general purpose/normal resolution algorithm. The phase content and crystallinity of the $MAPbI_3$ thin films were checked by x-ray diffraction (XRD) on a Bruker D8 Discover with CuKα tube, parallel mirror optics, 0.6 mm divergence slits, and a scintillation detector.

Photovoltaic Device Fabrication and Characterization

Photovoltaic devices were fabricated on solvent cleaned and O_2 plasma treated patterned indium tin oxide (ITO) substrates. A thin (0.8 mg/mL in chlorobenzene) poly-TPD (American Dye Source, Inc.) hole transport layer (HTL) was spin coated onto the ITO. Following a short 2 s O_2 plasma treatment of the poly-TPD for wetting purposes, the MAPbI3 films were cast from 0.15 M DMF solutions at 4100 rpm. If a solvent exchange was performed, it was done at 4 s after the start

of spinning. The $MAPbI_3$ layers were dried for 5 minutes at 65°C. A C_{60} (Nano-C, purified) electron transport layer (HTL) was evaporated followed by 9 nm of bathocuproine (BCP) (Nichem, purified) and then 100 nm of Al through a shadow mask to define a device area of 0.1 cm^2. The device performance was characterized inside of an N_2 filled glovebox by current-voltage measurements sweeping both forward (-1 to 1.25 V) and reverse (1.25 to -1 V) scans with a Keithley 2602B source-measure unit. The devices were illuminated with AM1.5G using an ABET Technologies solar simulator attached to the glovebox and calibrated with a Si reference cell. The devices showed non-negligible but reproducible hysteresis. The measurement script was designed to hold the device at the starting voltage (either -1 V for forward or 1.25 V for reverse scan) for 1 s prior to sweeping at ~0.1 V/s to exacerbate rather than mitigate the hysteresis. Three of each sweeps were measured to pseudo-stabilize the device, the third of which were used for the device parameter statistics.

Supplementary Figures

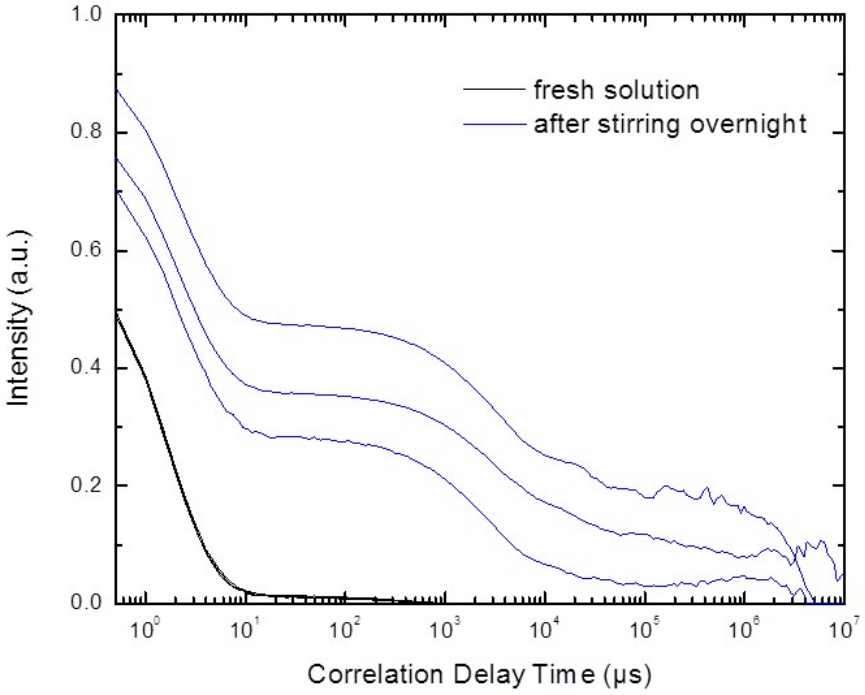

Figure S1. Correlogram from the DLS measurements on a 33 wt% solution of PbI_2:MAI ratio 1:1 in DMF. The mother solution was stirred until dissolved and then filtered. Measurements were performed on aliquots taken from the mother solution within an hour of filtering and after stirring overnight.

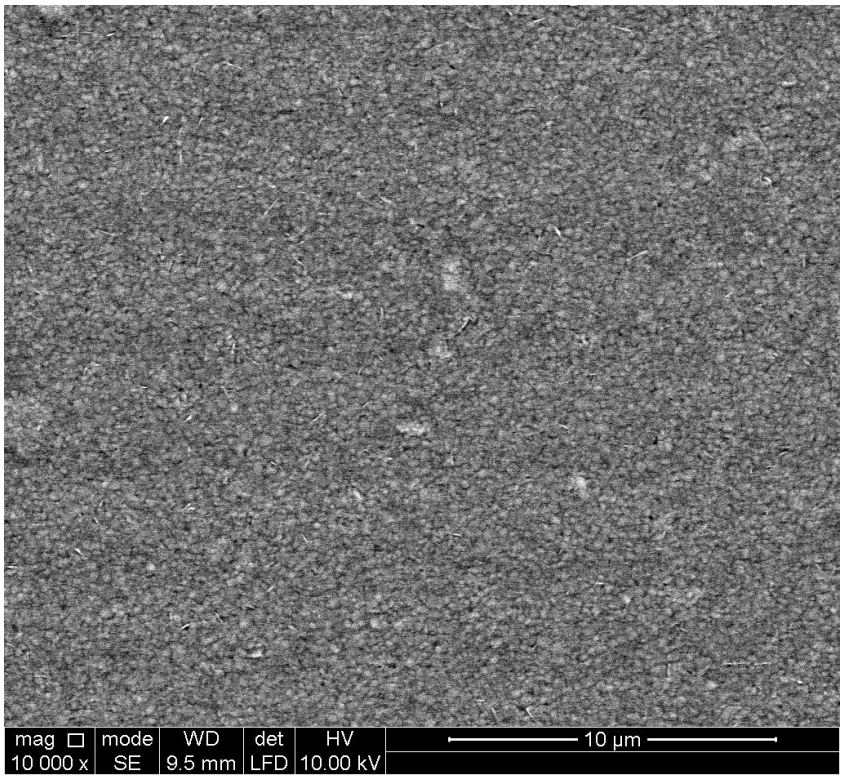

Figure S2. Large area SEM image of an $MAPbI_3$ film cast from 0.75 M solution with toluene solvent exchange at 4 s showing that the film is continuous and uniform over very large areas.

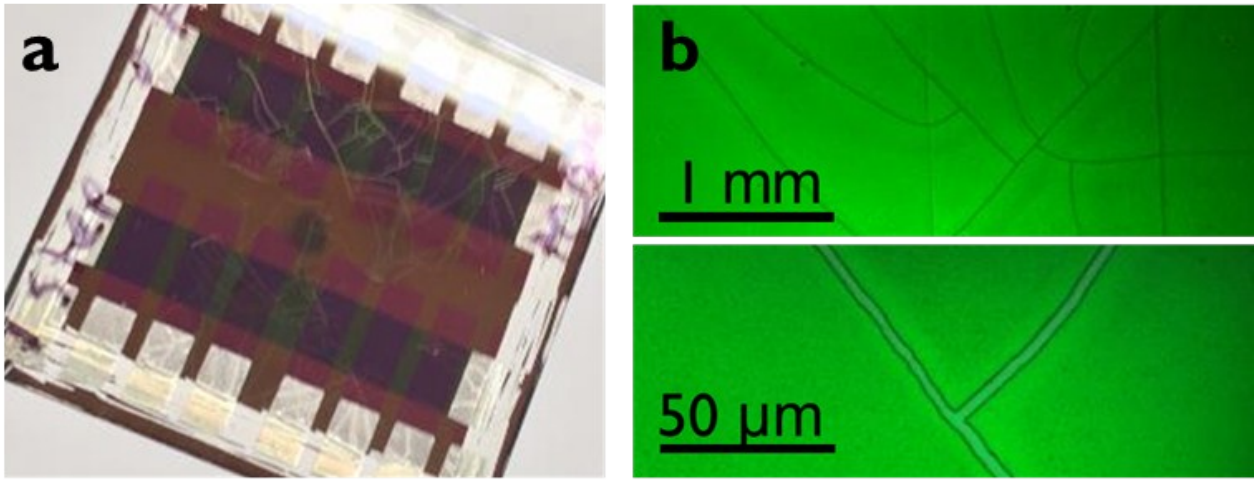

Figure S3. Photograph (a) and optical micrographs of cracked of films of $MAPbI_3$ when attempting to fabricate very thick (> 500 nm) layers for photovoltaic devices.

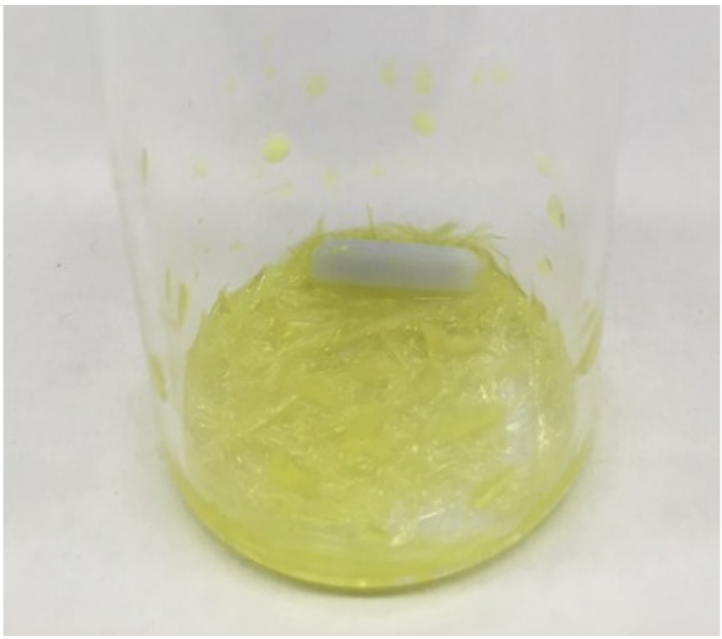

Figure S4. Photograph of supersaturated PbI_2:DMF solution after storage for a few hours. Large needle-like crystals precipitated out of the colloidal solution and protrude out from where the surface of the liquid once was.

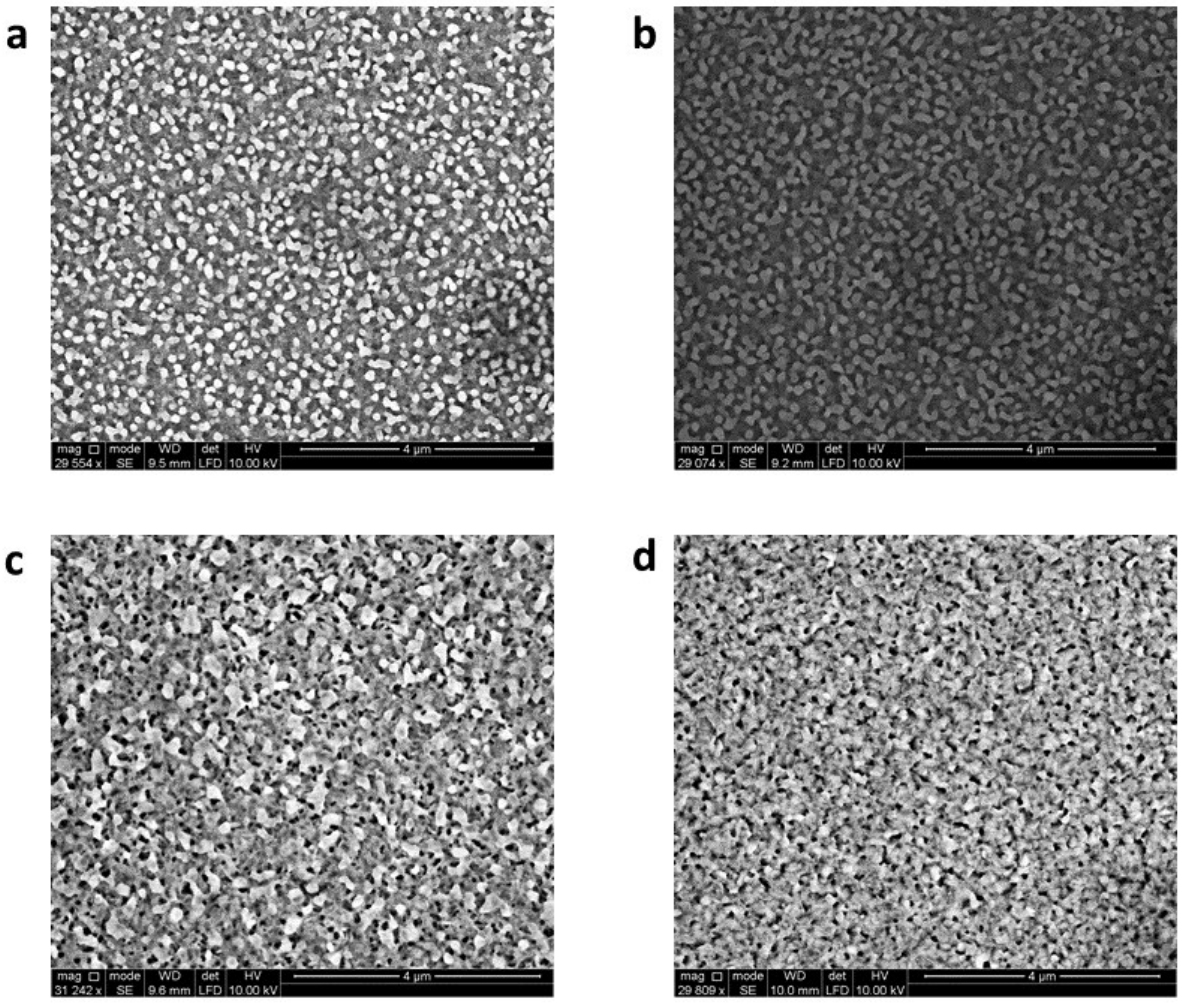

Figure S5. SEM images of PbI_2 films deposited in a saturated DMF atmosphere and solvent exchanged at (a) 4 s, (b) 5 s, (c) 7 s, and (d) no solvent exchange.

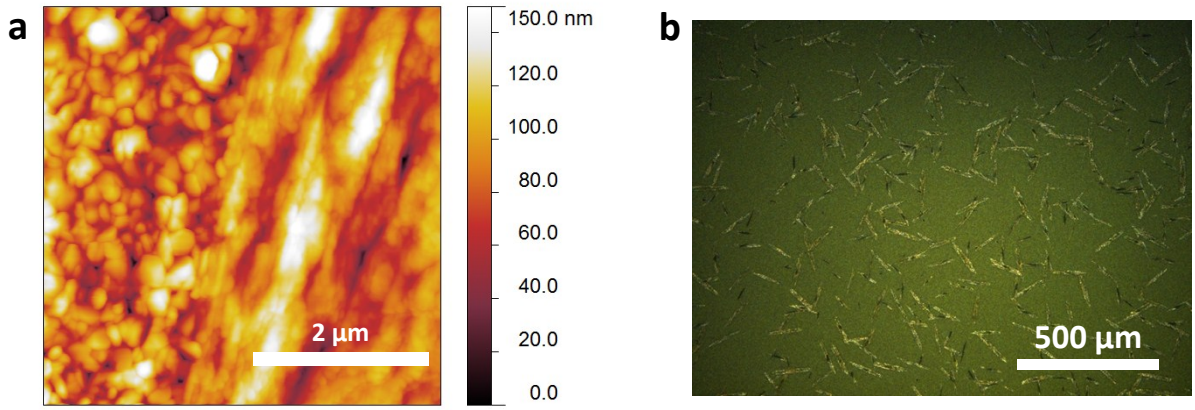

Figure S6. PbI_2 film spun in a saturated DMF atmosphere and exposed to the DMF vapor for 3 minutes after spinning. AFM image (a) and dark field optical micrograph (b) show the formation of macroscopic needle features on the film surface due to the DMF exposure. The right side of the AFM image is on one of the needles shown in (b). The needle-like features are clearly not a single crystal.

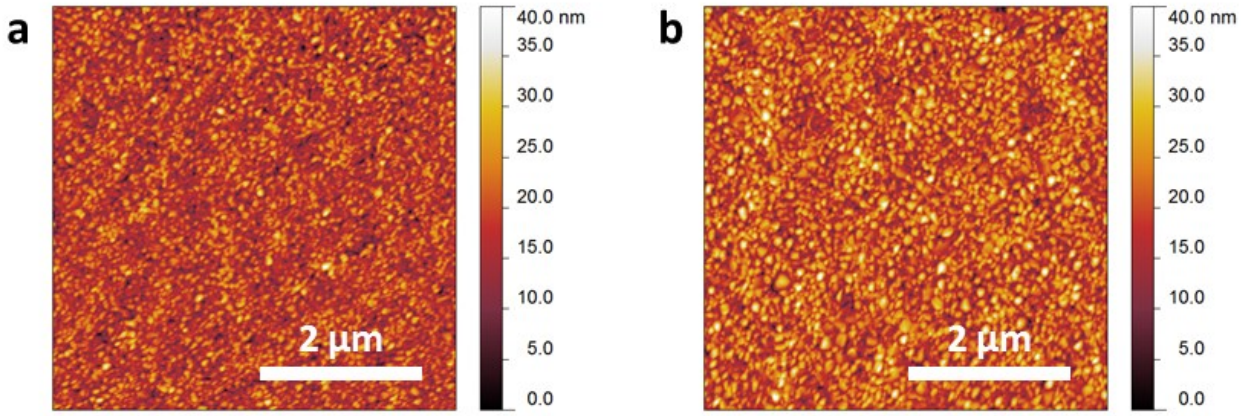

Figure S7. AFM of $MAPbI_3$ films spun cast from 33 wt% solution at (a) 5500 rpm and (b) 3500 rpm in a low DMF vapor pressure environment with solvent exchanges at optimal times of 4 s and 7 s, respectively. Spinning at slower speeds allows particles to grow for a longer period of time resulting in a larger average grain size.

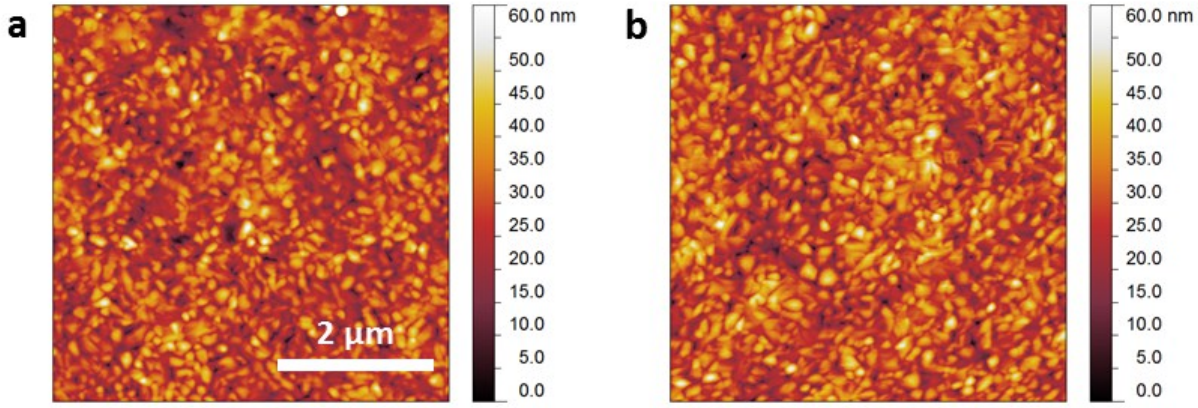

Figure S8. AFM of $MAPbI_3$ films spun cast from 54 wt% solution at 6500 rpm in a low DMF vapor pressure environment with solvent exchanges at (a) 4 s and (b) 5 s. The root mean square (RMS) roughnesses are both ~7.5 nm.

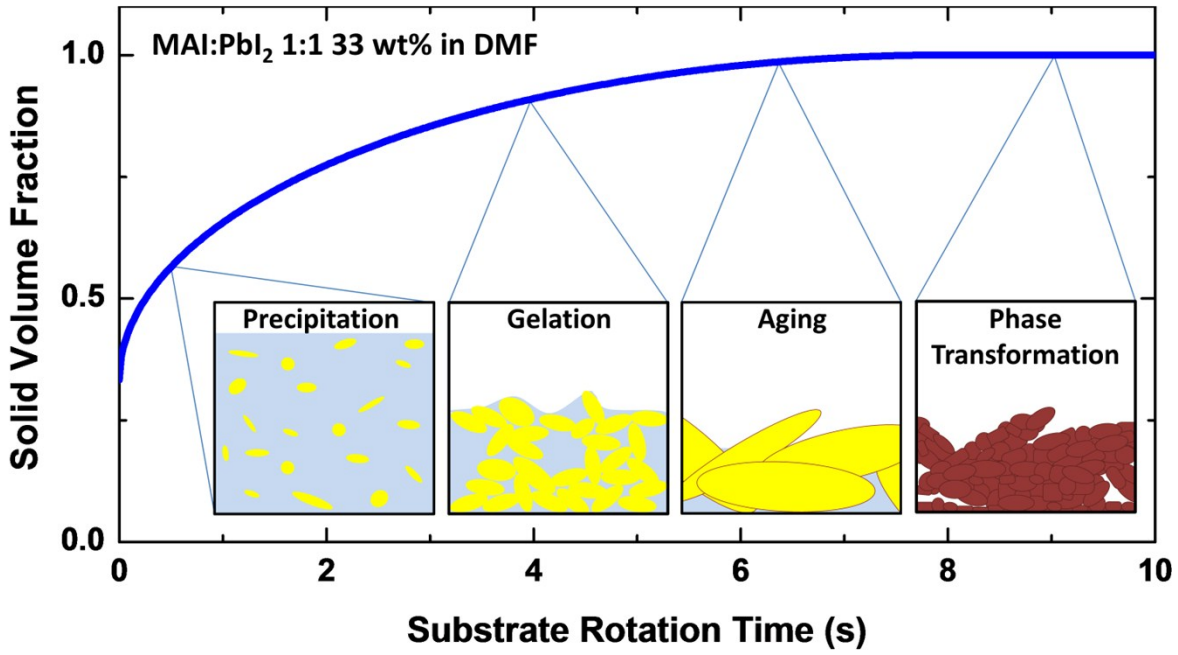

Figure S9. Schematic illustrating the evolution of a stoichiometric solution of MAI:PbI2 showing the gelation kinetics in real time during a spin coating process (5500 rpm) in the *absence of a solvent exchange*. At first, PbI_2 particles coordinated strongly by MAI and DMF form as the solution becomes supersaturated. The film has gelled at 4 s and then rapidly ripens into large particles that give the film visible haze. These particles then eject DMF as it continues to dry, decomposing into many $MAPbI_3$ grains patterned into needles by the large MAI:DMF:PbI_2 crystals. If a solvent exchange is performed at 4 s to remove the DMF, the ripening cannot occur because the solid is no longer soluble in the exchanged solvent and the rapid removal of DMF also converts the particles to $MAPbI_3$ instantly, leaving a smooth perovskite ambigel or xerogel.

Film Cracking

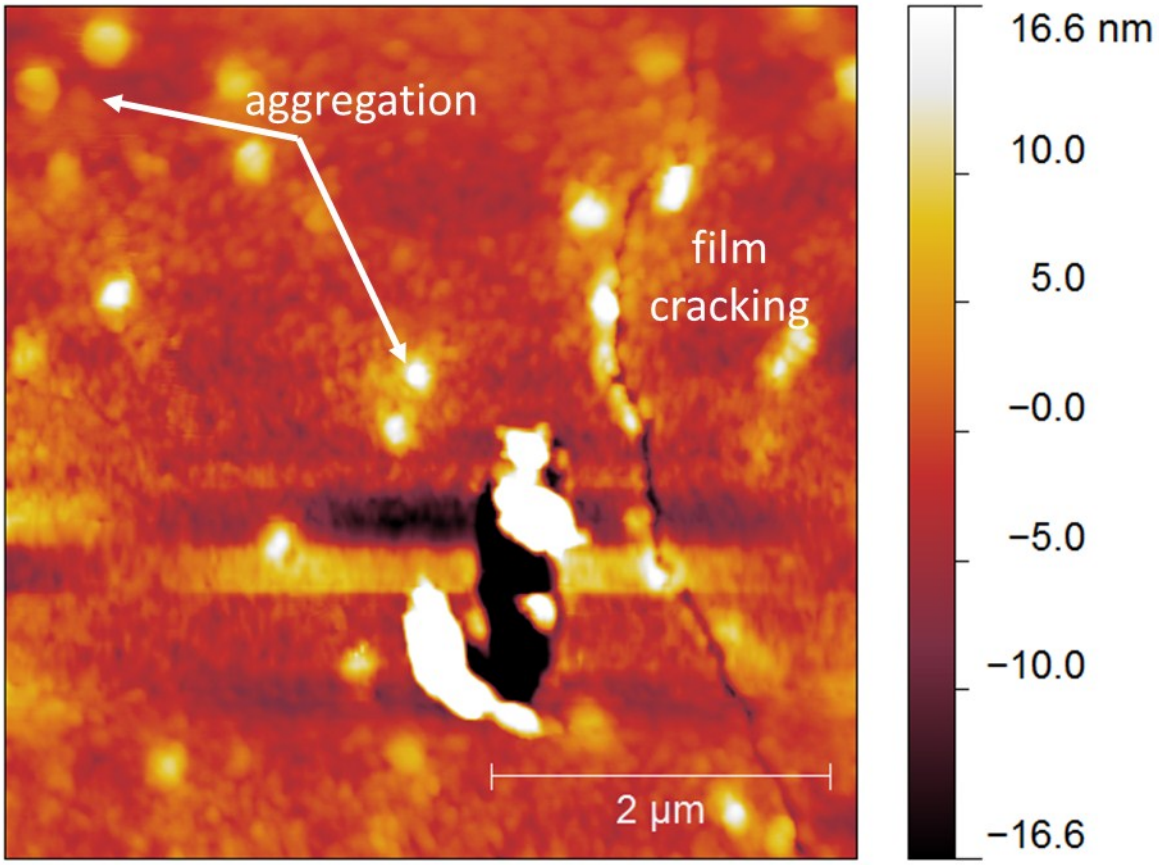

Figure S10. Micro/nano scale cracking is still observed on some areas of the substrate via AFM of 0.3 M $MAPbBr_3$ solutions with no additives on glass substrates.

Microcracking of 0.3 M concentrations for $MAPbBr_3$ (no additive) indicate that the thickness threshold for cracking is less for $MAPbBr_3$ than for $MAPbI_3$. Well controlled surface morphology were observed for $MAPbBr_3$ films made from solutions of < 0.3 M. The many "peaks" on the surface are due to aggregation in solution or surface aggregation as depicted in Figure 2b in the main article. Below the critical thickness, these aggregates are not present when the solvent exchange is performed at 4 s, similar to the $MAPbI_3$ situation.

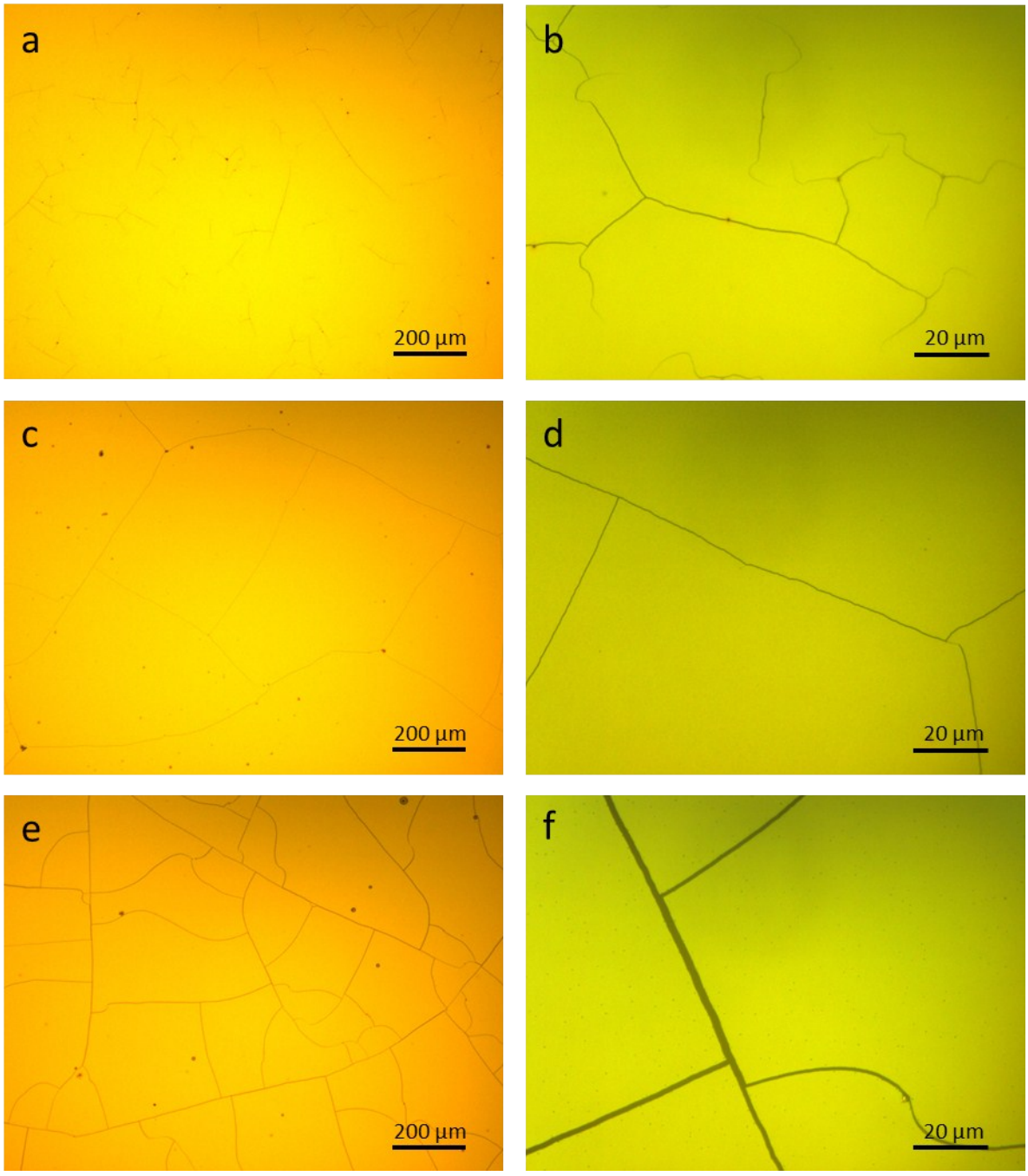

Figure S11. Optical microscopy of toluene exchanged (at 4 s) $MAPbBr_3$ thin films with no additive (a,b), BABr:MABr = 0.1 (c,d), and BABr:MABr = 0.2 (e,f) spun from 0.3 M solutions on poly-vinylcarbizole (Sigma Aldrich, cast from chlorobenzene) coated glass substrates.

Thin films will crack when the volume of stress (energy per unit volume) is greater than the energy required to form two new surfaces (twice the free surface energy) which only occurs for sufficiently thick films.[2] This critical cracking thickness was large for $MAPbI_3$ (> 450 nm) and does not prevent the fabrication of thick absorbing layers via a solvent exchange. In contrast, $CsPbBr_3$ and $MAPbBr_3$ films cracked at much lower thicknesses. It was observed in $MAPbBr_3$ films near the critical cracking thickness of the control (0.3 M solutions) display interesting cracking properties. The crack width as well as connectivity/density increase as the BABr additive concentration increases. This is well supported by sol-gel theory. The Young-Laplace equation says that capillary stresses will be inversely proportional to the pore radius. The XRD data support that the BABr addition decreases the particle size. Assuming that the pore size also decreases as the particle size decreases, higher stresses and degrees of cracking should occur in the films with smallest particle size, which is clearly observed in Figure S10. The solvent exchange technique is therefore less technologically applicable for device fabrication employing $MAPbBr_3$ as continuous films are limited to < 150 nm depending on substrate surface energy.

Table S1. Photovoltaic parameters of thin $MAPbI_3$ solar cell devices under 100 mW/cm² AM1.5G simulated solar illumination. The third forward and reverse scans are presented for each device. Standard deviations are in parentheses. The champion device for BAI + SE + 10 nm C_{60} had a PCE = 6.0 and 6.6 % in the forward and reverse directions, respectively.

C_{60} thickness (nm)	$MAPbI_3$ Layer Treatment*	Scan	V_{oc} (V)	J_{sc} (mA/cm²)	FF	PCE (%)	# of devices
25	BAI + SE	fwd	1.07 (0.01)	7.6 (0.2)	0.60 (0.03)	4.9 (0.2)	12
	BAI + SE	rev	1.08 (0.01)	7.6 (0.2)	0.70 (0.02)	5.8 (0.1)	
25	no additive + SE	fwd	0.69 (0.02)	9.7 (0.3)	0.56 (0.03)	3.8 (0.3)	24
	no additive + SE	rev	0.72 (0.03)	9.8 (0.3)	0.62 (0.02)	4.4 (0.3)	
25	BAI	fwd	0.6 (0.02)	9.5 (0.1)	0.407 (0.07)	2.3 (0.1)	12
	BAI	rev	0.73 (0.01)	9.8 (0.1)	0.582 (0.006)	4.2 (0.1)	
25	no additive	fwd	0.706 (0.009)	10.6 (0.2)	0.655 (0.005)	4.9 (0.2)	11
	no additive	rev	0.72 (0.01)	10.73 (0.08)	0.672 (0.005)	5.2 (0.1)	
10	BAI + SE	fwd	1.07 (0.02)	8.2 (0.2)	0.61 (0.08)	5.3 (0.8)	12
	BAI + SE	rev	1.08 (0.02)	8.1 (0.2)	0.68 (0.05)	6.0 (0.5)	
10	no additive + SE	fwd	0.61 (0.06)	10.1 (0.6)	0.51 (0.09)	3 (1)	12
	no additive + SE	rev	0.65 (0.03)	10.3 (0.4)	0.56 (0.08)	3.8 (0.8)	

*All active layers were cast from 0.15 M $MAPbI_3$ solution in DMF. Films containing the additive are denoted BAI and films for which a solvent exchange was performed are denoted SE.

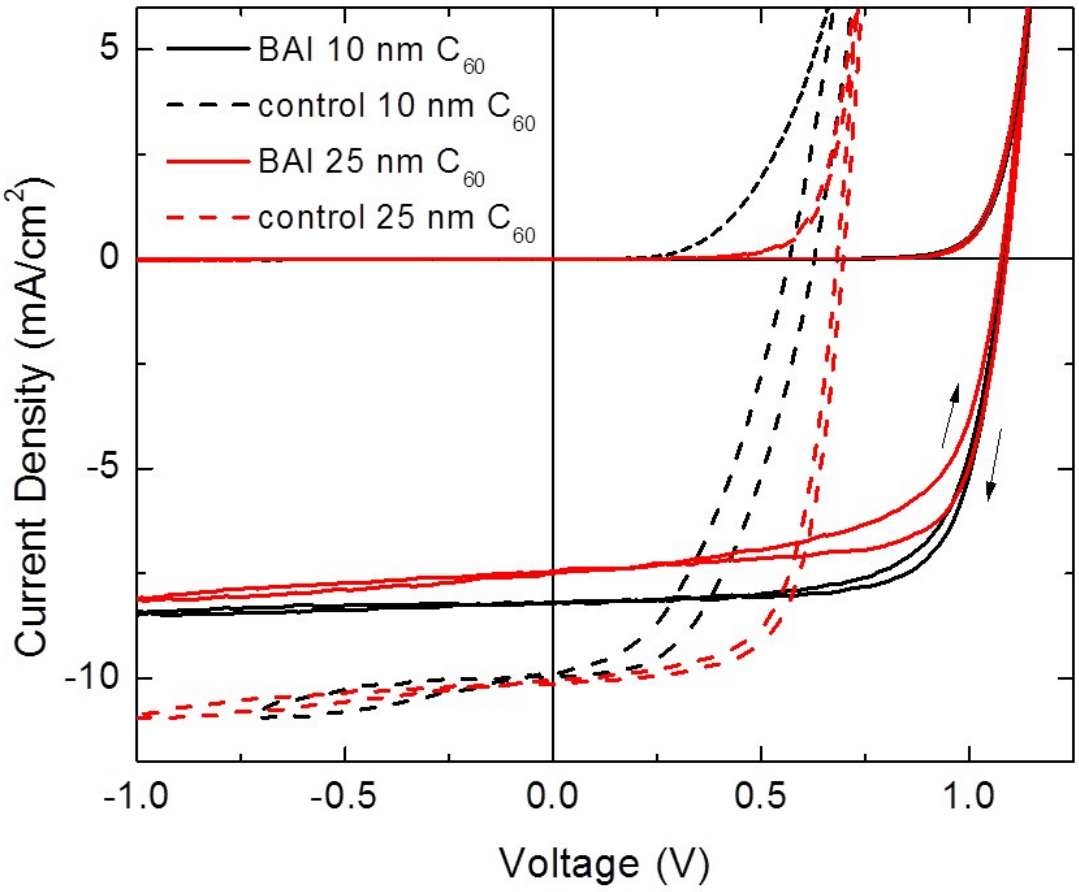

Figure S12. *J-V* characteristics of photovoltaic devices employing ~ 30 nm thick solvent exchanged $MAPbI_3$ with and without BAI additive. The red curves have 25 nm of C_{60} as an ETL while black lines have only 10 nm of C_{60}. It is clear that the superior quality of the BAI additive films allow the maximum V_{oc} for this material to be achieved in an incredibly thin device. The extremely low surface roughness also allows for thinner ETLs, reducing contact resistance and maximizing charge collection efficiency. The dark curves are also shown.

References

1. N. J. Jeon, J. H. Noh, Y. C. Kim, W. S. Yang, S. Ryu, and S. Il. Seok, *Nat. Mater.* 2014, **13**, 897–903.
2. M. A. Meyers, K. K. Chawla, and W. F. Hosford. *Mechanical Behavior of Materials, Ed. 2*, Cambridge University Press, 2008, chapters 7-8.